Astron. Astrophys. 326, 632–639 (1997)

ASTRONOMY
AND
ASTROPHYSICS

New multiple young stellar objects discovered by near-infrared speckle imaging

N. Ageorges[1], **A. Eckart**[2], **J.-L. Monin**[3], **and F. Ménard**[3]

[1] ESO, Karl Schwarzschild Strasse 2, D-85748 Garching bei München, Germany
[2] Max Planck Institut für Extraterrestrische Physik (MPE), Giessenbachstrasse, D-85748 Garching bei München, Germany
[3] Laboratoire d'Astrophysique, Observatoire de Grenoble, Université Joseph Fourier, BP 53X, F-38041 Grenoble Cedex 9, France

Received 2 December 1996 / Accepted 20 May 1997

Abstract. We present the results of a near infrared high angular resolution study of young stellar objects. The observations have been carried out in 1993 and 1994 with the speckle camera SHARP 1 installed at the ESO-NTT. The sources were selected because of their known high degree of polarization at optical wavelengths, in order to search for disk-like extended structures. This paper only concentrates on the new multiple systems discovered. After a general presentation of the sample, each new system is presented individually. Then the relative reddening of the individual components as well as the possible link between the morphology of a system and its polarization are discussed.

Key words: polarization – circumstellar matter – stars: formation – stars: imaging – stars: pre-main sequence – infrared: stars

1. Introduction

A full understanding of star formation requires one to study the interaction of the central object with its accompanying environment. Undoubtedly, the interaction of the central core with its immediate surroundings is of prime importance in determining the final physical properties of the star.

High angular resolution (HAR) can be used to determine the multiplicity of stars (i.e. invoking different scenarios of star formation), to study the distribution and properties of circumstellar matter, to pick out objects in a crowded field (like in the Galactic Center), and to do high sensitivity searches for faint sources (e.g. detection of disks, or faint companions). The use of HAR techniques to observe young stellar objects (YSOs) corresponds to the goal of detecting and resolving disk-like structures (well expected features of young stars) around these sources.

The near-infrared (NIR) is well-suited for the study of the circumstellar environment of YSOs since, at these wavelengths, the optical depth is ten times smaller than in the visible and the obscuration of the star thus lower. The NIR is indeed adapted to study YSOs deep in molecular clouds because extinction is lower; but lower extinction also means that the circumstellar medium is optically thinner and the scattering efficiency is lower. As a consequence the circumstellar medium will appear smaller or will not be detectable at all. From that point of view near infrared observations in the J band are preferred to observations in the K band.

For this study, we have selected YSOs known to have a high degree of polarization at optical wavelengths (observations with PISCO). This survey, realized with the MPE speckle SHARP (System for High Angular Resolution Pictures) camera, has been done in the southern hemisphere and covers the LST range from 10:00 to 22:00 hours. The sample is not biased towards membership in any clouds or associations.

The initial idea was to look for disks since the degree of polarization of YSOs is interpreted, within the framework of multiple scattering (see e.g. Bastien & Ménard 1990), in terms of extended asymmetrically distributed matter around the source (Bastien & Landstreet 1979). However, no disks were found. Two main reasons could be invoked to explain this non-detection: the signal-to-noise ratio reached might have been too small and/or the disk might be much smaller than expected. Those points will not be discussed further here; but the following parts do report on new multiple systems discovered.

We present here the results of two observing runs conducted in 1993 and 1994. The details of the observations are presented in Sect. 2 together with the reduction procedure. Sect. 3 presents the newly discovered multiple systems individually. The results of this study, as well as their impact on the selection criteria are discussed in Sect. 4.

2. Observations

In July-August 1993 and April-May 1994, we obtained high angular resolution speckle images of the YSOs listed in Table 1, at near infrared (NIR) wavelengths (between 1 and 2.5 μm). This survey has been conducted at the ESO-NTT, using the MPE SHARP 1 camera (Hofmann et al., 1995). This NIR speckle camera is equipped with a Rockwell NICMOS 3 $(256)^2$ pixel

Send offprint requests to: N. Ageorges at ESO

array. It has been designed to obtain diffraction-limited images at 2.2μm (K band) at the NTT, i.e. a resolution of 0.15″. The pixel size on the sky is 0.05″. The effective resolution reached at J(1.25 μm) and H(1.65μm) is about 0.1″. The resolution we obtained reliably in the final images, in K-band, is close to 0.2″ and close to the NTT diffraction limit. The data reduction was carried out using the IRSI speckle interferometry package (Eckart & Duhoux 1990).

For each source, a neighbouring point-like SAO star has been used to determine the Point Spread Function (PSF) in order to deconvolve the data, once they had been corrected for the sky contribution, flat field effects and dead pixels. The diffraction-limited imaging in almost all cases was carried out using the Simple Shift-and-Add (SSA), a Knox-Thomson deconvolution and the simple power spectrum deconvolution followed by a Fienup algorithm. For the other sources, the same procedure was used but the diffraction limit could not be reached reliably.

We have done quick-look on-line observations to search for large separation (10″) companions. Therefore, we positioned the target object at the 4 corners of the maximum field-of-view (12.8″$\times$ 12.8″) of the camera to detect any companion brighter than 10^{th} magnitude, in an effective area of 20″$\times$ 20″. This magnitude corresponds to the detection limit of a star in a single exposure frame for a typical integration time of about 0.5 sec with a seeing between 0.5″ and 1″. This is our detection limit for large separation companions since this systematic search has been done at the telescope and no frames have been recorded during this search.

Each double source has been observed at J, H and K in order to get photometric information. For this purpose, flux densities have been determined in small apertures of similar size. Accurate absolute flux densities (i.e. magnitudes) could be derived for only seven of the observed binary systems (primarily due to a lack of good flux calibrators); for the others we determined relative photometry.

The sources are described in Table 1, which begins with the name of the object and its coordinates. Column 3 indicates if the source is unresolved, extended, binary or multiple (more than 2 components). In the case of multiple systems, the separation and position angle are given, relative to the primary, in column 4. Then the polarization values are listed. The last column indicates the class of objects to which the source belongs (i.e. T Tauris – TTS – or Herbig Ae/Be stars – HAEBE –).

Field orientation and plate scale were checked against the well calibrated galactic center, every night. The orientation is, to within an accuracy of 1°, north to the top and east to the left and the plate scale is 50 mas to within better than 2% (Eckart & Genzel 1997, Menten et al. 1997). In the following, we assume that for all observational epochs, the camera was always aligned such that north is to the top and east to the left and the pixel scale was 50 mas.

The polarization data were obtained with PISCO, the 2-channel Polarimeter with Instrumental and Sky COmpensation, attached to the ESO/MPI 2.2m telescope, located in La Silla, Chile, during the period of May 22 to 27 1992. For a complete description of the instrument see Schwarz (1989).

All the data presented here were obtained through a 9.″7 diaphragm, and a standard Johnson I filter. Instrumental and sky polarizations were evaluated after compensation by PISCO, and found to be negligible. The instrumental efficiency and position angle zero-point were checked and corrected every night by measuring well-known polarized standard stars (e.g., Bastien et al. 1988). In addition the instrumental efficiency was further evaluated every night by inserting a polaroid sheet in the beam. All values in column 5 (P in%) and 6 (θ in degrees) in Table 1 are corrected for these effects.

A polarimetric study of the CTTS versus WTTS population in the southern hemisphere (Ménard, 1997, in preparation) will fully exploit the polarization data.

3. Results

Of the multiple systems observed in this study, we elaborate only on the six that are new discoveries.

3.1. Comments on the complete sample

From the 28 objects observed (see Table 1), 12 are point sources at our sensitivity and resolution of $\leq 0.2''$. Some of these sources are actually very close binaries (like ROX 14; Simon et al. 1995). Over the 4 extended objects, Parsamian 21 and 1548C27 were already known to be reflection nebulae. WSB 16, observed in H band under a seeing of 0.7", presents a small North-West elongation: 95% of the flux is contained within 1″. The last extended object observed, V536 Aql, is also a binary, which has been extensively discussed in Ageorges et al. (1994) and Ageorges & Duschl (1996) and will therefore not be further mentioned here.

The twelve other stars are multiple. Half of them were already known, see references given in the caption of Table 1. They will not be discussed here as well. We now present each new multiple system in detail.

3.2. CHX 6B

This source is one of the candidate optical counterparts for the X-ray source number 6 in the Chamaeleon I dark cloud (Feigelson & Kriss 1989). It is a reddened M0 star with a V magnitude of 14 and without prominent emission lines. Walter (1992) classifies this WTTS with W(Hα) = 1.1 Å as a giant of spectral type M1.

We observed CHX 6B in April 1994 in H-band and July 1995 in K-band. The mean seeing for the K band observations was 0.65″. Due to the weakness of the source, this resolution could only be improved marginally by shift-and-add algorithm ($\approx$ 0.55″) and diffraction limit could not be reached. Nervertheless we found two companions of this source (Fig. 1), which is a very good example of the quality of the results we can obtain. Indeed, the intensity ratio between the main and secondary components is 550, which corresponds to a Δm_K of $\approx$ 6.85! The separation is 2.45$\pm$0.05″ at 48.6$\pm$0.5°. The secondary component itself is binary. The third component is at a distance of 0.2$\pm$0.05″ from the secondary at a position angle of 226.4$\pm$1.5°. In Table 1 we

Table 1. List of observed objects. In the case of triple star system, the position of the tertiary component is measured with respect to the primary. The polarization measurements for V 536 Aql and 1548 C 27 have been achieved at 0.7μm and not at 0.9μm like the rest of the survey. Meaning of the abbreviations used: 'ps' = point source, 'b' = binary, 'e' = extended source, 'ms' = multiple system. References: (1) Chelli et al. 1988; (2) Simon et al. 1987; (3) Mathieu et al. 1989; (4) Reipurth & Zinnecker 1993; (5) Ageorges et al. 1994; (6) This study

N°	Source	Remark	δ" ($\pm$)	PA^o ($\pm$)	P(%)	$\theta(^o)$	Nature
1	SZ Cha	b	5.20 (0.025)	145.5 (0.5)	4.31 (0.08)	131.3 (1.0)	WTTS
2	LHα 332-20	ps			3.63 (0.19)	125.6 (1.5)	CTTS
3	Hm 10	ps			4.50 (0.07)	109.1 (1.0)	
4	CHX 6B	ms (6)	2.45 (0.05)	48.6 (0.5)	4.67 (0.09)	115.9 (1.0)	WTTS
			2.25 (0.05)	48.8 (1.5)			
5	CED 110	ps			2.82 (0.13)	104.8 (1.3)	WTTS
6	Sz 21	ps			3.59 (0.08)	132.4 (1.0)	TTS
7	CHX 10A	ms (6)	1.86 (0.025)	118.4 (0.2)	4.03 (0.05)	149.2 (1.0)	WTTS
			1.96 (0.05)	122.8 (5)			
8	Haro 1-1	ps			2.93 (0.17)	172.6 (1.6)	TTS
9	WSB 16	e (6)			2.36 (0.27)	160.4 (3.3)	
10	ROX 5	b (6)	0.13 (0.05)	130 (2)	2.47 (0.08)	32.9 (1.0)	WTTS
11	ROX 7	ps			4.11 (0.04)	174.4 (1.0)	WTTS
12	Do-Ar 21	ps			5.81 (0.09)	1.6 (1.0)	WTTS
13	Do-Ar 24E	b (1)	2.06 (0.025)	331.4 (0.5)	4.58 (0.15)	179.9 (1.0)	WTTS
14	ROX 14	ps			7.13 (0.17)	25.8 (1.0)	
15	Do-Ar 32	b	10.06 (0.04)	332.1 (0.5)	5.31 (0.08)	39.7 (1.0)	CTTS
16	ROX 30C	ps			3.67 (0.09)	25.5 (1.0)	CTTS
17	ROX 16	b	0.59 (0.04)	104.6 (1)	4.07 (0.13)	30.5 (1.0)	CTTS
18	ROX 31	b (2)	0.39 (0.025)	71.6 (0.1)	4.88 (0.12)	56.4 (1.0)	WTTS
19	ROX 39	ps			2.60 (0.16)	31.4 (1.8)	WTTS
20	ROX 42 B	ps			2.72 (0.03)	15.1 (1.0)	WTTS
21	ROX 43 A(B)	b (3)	4.67 (0.1)	13.7 (0.1)	2.63 (0.04)	16.5 (1.0)	WTTS
22	MWC 300	ps			4.27 (0.06)	57.2 (1.0)	HAEBE
23	AS 310	ms (6)	see Table 2				HAEBE
24	R CrA	ps			6.43 (0.03)	5.8 (1.0)	HAEBE
25	VV CrA	b (4)	2.08 (0.025)	46.85 (0.12)	3.81 (0.03)	115.0 (1.0)	CTTS
26	Parsamyan 21	e					HAEBE
27	V 536 Aql	b + e (5)	0.52 (0.025)	16.7 (0.2)	8.35 (0.30)	39.6 (1.0)	TTS
28	1548 C 27	e			6.36 (0.36)	172.5 (1.5)	

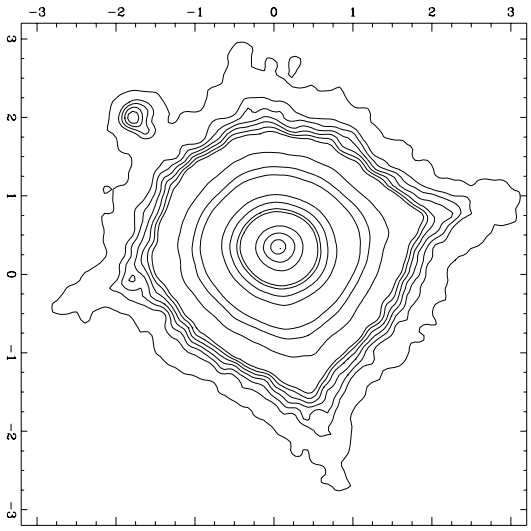

Fig. 1. K band SSA image of CHX 6B (6.4" × 6.4"). The orientation is the same for all figures: North is up and East to the left.

give the position of the tertiary component data with respect to the primary. 200 frames have been acquired in the K band, where the multiplicity of the system appears at best. We need more data to correctly deconvolve the images. Absolute calibration of this source was not possible since no suitable flux calibrator was observed during the night of these observations.

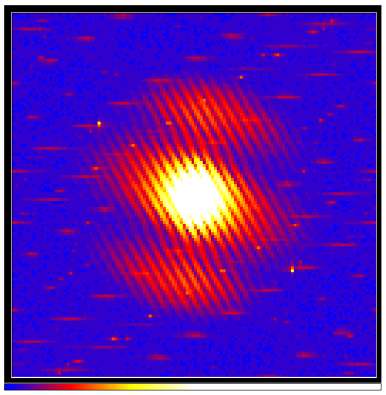

Fig. 2. Power spectrum of CHX 10A pointing out the multiplicity (3 stars) of this system

3.3. CHX 10A

The SSA images of this source, resulting from the April 1994 observations, are clearly characteristics of a binary system, but the power spectrum (see Fig. 2) tells us more: it points out the existence of a third component. A detailed study of each component of this system shows that the southernmost star is a binary. The separation between the primary and the secondary is 1.86$\pm$0.025$''$ at 118.4$\pm$0.2° and the faintest star is located at 0.18$\pm$0.05$''$ from the secondary at a position angle of 175$\pm$5°. In Table 1 the position of the two companions of CHX 10A are indicated with respect to the primary.

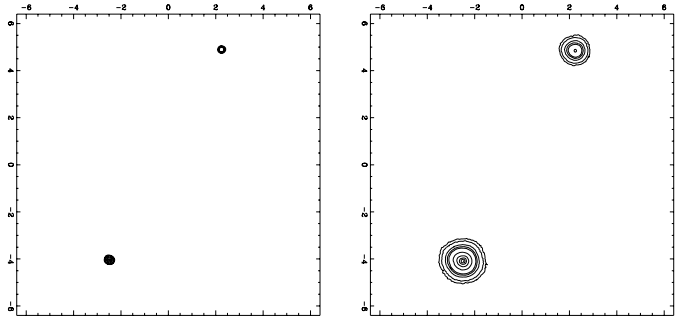

Fig. 3. Do Ar 32. Right: J band SSA image (Contour levels are at 1.3 (4σ), 2, 4, 6, 8, 20, 40, 60, 80 and 100% of the intensity peak.). Left: H band linear deconvolved image (Contour levels are at 3 (4σ), 5, 8, 10, 30, 50, 80, 100% of the intensity peak)

3.4. Do Ar 32

We found a companion (Fig. 3) to the pre-main sequence star Do Ar 32 (CTTS, André & Montmerle 1994; spectral type K4, Bouvier & Appenzeller, 1992) at $10.06'' \pm 0.04''$ at a position angle of $332.1 \pm 0.5°$. This detection does not require high angular resolution but the binarity of the source has nevertheless never been mentioned previously in the literature.

In this case, it is clear that the degree of measured optical polarization quoted in Table 1 corresponds to measurements of one of the components only, the brighter one at optical wavelengths, since the diaphragm used for the polarimetric measurements is of $9.7''$.

For this source, more than for any others, the question of the association of the two components as one physical system is crucial, since it is our largest separation binary. As in the study of Leinert et al. (1993), the largest separation to be found in our survey is not given by physical limits on angular momentum but by the ability to recognize a companion among foreground and background stars. In the case of Do Ar 32, insufficient information exists precluding any firm conclusions. Observations at different epochs as well as spectroscopy will be needed to determine the distance of the sources and their relation to each other.

3.5. ROX 5

ROX 5 has been detected by X-ray observations with the Einstein satellite (Montmerle et al. 1983). We have observed it in H band in April 1994 with a typical seeing of $0.65''$. The resolution in the SSA image is of the order of $0.25''$. The reference star observed appears point-like, however our deconvolved images of ROX 5 present an elongation over 2-3 pixels at a position angle of $\approx 130°$. The explanation is to be found in the power spectrum of this source (Fig. 4), which reveals that this is a binary system with a separation of $\approx 0.13''$. The elongation seen in the deconvolved images characterizes the difficulty in reconstructing an image of such a close binary near the diffraction limit ($0.12''$ in the H band) with a $0.05''$/pixels sampling. Nevertheless the binary nature clearly shows up in the power spectrum

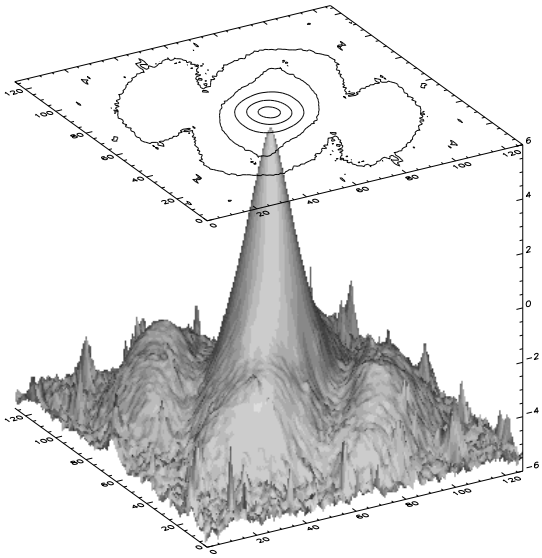

Fig. 4. Power spectrum of ROX 5, rotated by 90 degrees for the presentation. Contour levels are at 0.5, 1, 4, 7, 20,40, 70 and 100% of the intensity peak

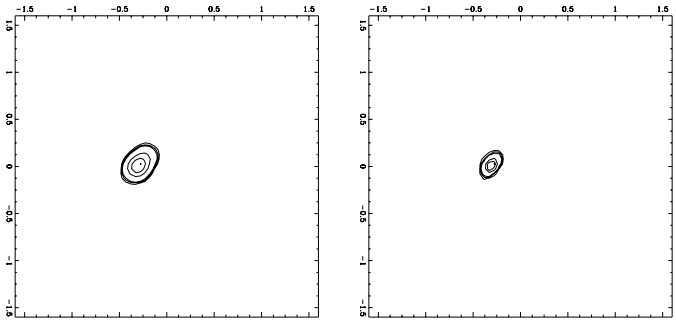

Fig. 5. Deconvolved images of ROX 5 (3"×3"). Contour levels are at 4, 7, 10, 40, 70 and 100% from the intensity peak. Left: Lucy deconvolved images; right: linear deconvolved images, from the SSA images, followed by 200 Fienup iterations (gain loop of 0.3).

(Fig. 4 left) and the two deconvolved images (Fig. 5). The relative brightness of the sources must be of the order of 1:2 at most, corresponding to $\delta m_H \leq 0.75$.

3.6. ROX 16

This system has been resolved for the first time by our observations in April 1994 (Fig. 6). The projected separation is $0.59 \pm 0.04''$ at a position angle of $104.6 \pm 1°$. Vrba et al. (1976) give an optical polarization (at 0.5μm) of $3.78 \pm 0.1\%$ at a position angle of 39 ± 1^o. The degree of polarization measured at 0.9μm (see Table 1) is 4.07% at 30°. This small difference in the measurements can be interpreted in terms of the normal interstellar polarization wavelength dependence if the value of λ_{max} is large, e.g., ≈ 0.75 μm. This possibility is further supported by the similarity of the position angles of the average local interstellar polarization and the source's observed polarization. It is possible however that the source is also variable, a well es-

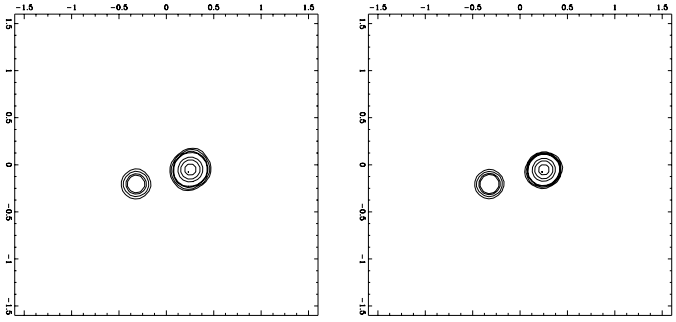

Fig. 6. H (left) and K band (right) linear deconvolved images of ROX 16 (3.2" × 3.2"). Contour levels are at 3, 5, 8, 10, 30, 50 80 and 100% of the intensity peak. The 3 σ level is at 2% in K band and 2.5% of the peak intensity in H band

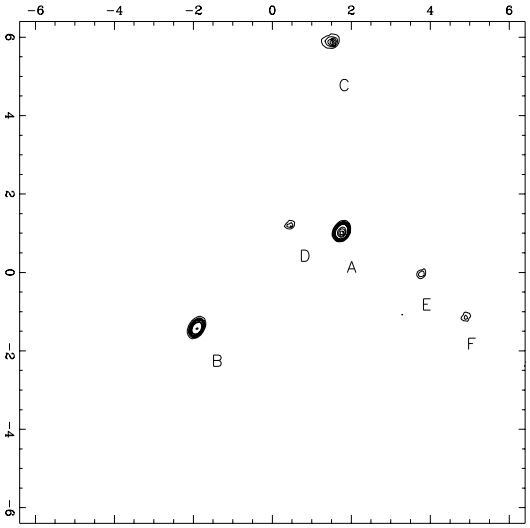

Fig. 7. Lucy deconvolved map (12.8" × 12.8") of AS 310 in K band. Levels are at 1, 2, 3, 4, 5, 8, 10, 30, 50, 80 and 100% of the image peak value, above the 3 σ level (= 0.7% of the peak intensity)

tablished behaviour for T Tauris (Ménard and Bastien 1992). Further polarimetric observations at different wavelengths are required to assess reasonnably if the origin of the polarization of ROX 16 is mostly interstellar or intrinsic. Furthermore the determination of the contribution of each component to the degree of polarization of the complete system should be determined.

3.7. AS 310

AS 310 is the only "cluster" discovered by this study. Up to now, it was known as a binary system (Bastian & Mundt, 1979; Finkenzeller & Mundt, 1984). It is associated with the HII region S61 and located at 2.5 Kpc (Georgelin & Georgelin 1970). Palla & Prusti (1993) discovered an H_2O maser associated with it, as often found in star forming regions. Hunter et al. (1990) used IRAS coadded survey data for locating IR sources within molecular clouds. The sources likely to be associated with the molecular cloud may also be connected with star formation continuing in other parts of the molecular cloud. Interestingly, within the accuracy of the IRAS and CO measurements, one of these sources is centered on AS 310.

Henning et al. (1994) measured a large 1.3mm continuum flux in a 23″ beam covering the whole region, corresponding to a gas mass of 30$M_\odot$. All these features suggest that AS 310 is located in a site where star formation is still active.

AS 310, ifself, seems to be a YSO (Hα emission often detected: Merrill & Burwell 1950; Cohen & Kuhi 1979; Stenholm & Acker 1987; Fich et al. 1990 and Goodrich 1993) embedded in a complex bright nebulosity. The presence of dust in the vicinity of this source is also suggested by the observations of Altenhoff et al. (1994). Indeed, they found a substantial emission at 250GHz in comparison to cm-observations (Skinner et al. 1993) and suggest that this extra flux density originates from thermal radiation of warm dust. Another hint of the youth of AS 310 is the discovery by Goodrich (1993) of two particular features which not only have different [SII]/Hα ratios than the rest of the nebula, but also show a morphology that is typical of jet flows near young stars. Those two features look morphologically similar to the heads of a bipolar jet centered somewhere near AS 310. They are situated only a few arcseconds away, on a direct line, in our high angular resolution image (Fig. 7), between C and A, if we assume that these objects originate from star A.

Table 2. Position angle, separation and magnitude difference of the different sources from the main source AS 310-A. Separations are given in arcseconds and position angles in degrees; error bars are in parentheses

Source	Separation (")	Position Angle (°)	δm_K ($\pm$0.05)
B	4.4 (0.1)	153.9 (0.2)	0.94
C	4.9 (0.1)	2.9 (0.2)	2.58
D	1.3 (0.1)	81.3 (0.2)	3.53
E	2.3 (0.1)	242.3 (0.2)	3.87
F	3.8 (0.15)	235.7 (0.3)	4.10

In the course of this survey, we discovered 4 more sources located close to the known binary. They are located in a 12.″8 × 12.″8 field (Fig. 7) around AS 310. The detected sources have been named according to their K magnitude, source A being the brightest. Sources A and B form the binary known before. The separation and position angle between each component and the brightest one are summarised in Table 2. Error bars are given in parentheses.

Our detection of a possible stellar cluster around AS 310 calls for further studies because embedded clusters associated with intermediate-mass Herbig AeBe stars are pivotal to understand the star formation mechanism(s). They represent the important transition between the high-mass stars that form with a multitude of low-mass objects around them, and the low-mass stars forming in relative isolation, in loose aggregates. Accurate near-infrared photometry and spectrosocopy is necessary to confirm the pre-main sequence nature and the physical parameters of this cluster.

Table 3. Magnitudes of binary systems ($\pm$ 0.2m) derived from the speckle observations. 'A' corresponds to the brightest source and 'B' its fainter companion

	Band	CHX 10 A	Do Ar 32	Do Ar 24E	ROX 16	ROX 31	VV CrA
	J	9.1	9.7	9.0	8.3	10.1	8.4
A,B	H		8.4	8.1	6.2	8.8	7.4
	K	7.9	7.8	7.0	6.1	8.2	5.8
	J	9.5	9.9	9.1	8.5		
A	H		8.7	8.3	6.4	9.4	7.7
	K	8.3	7.9	7.4	6.3	8.8	6.4
	J	12.8	11.5	12.1	10.4		
B	H		10.3	10.1	8.1	9.7	9.1
	K	9.1	9.8	8.2	8.2	9.1	6.7

4. Discussion

At our limiting magnitude ($m_K \leq 12$) and resolution ($\geq 0.2''$) twelve sources are point-like. They may however appear multiple at higher resolution (for example ROX 14, lunar occultations of Simon et al. 1995). We discuss now the results of our observations and their implications regarding the multiplicity, the colors and the polarization of the target sources.

4.1. Multiplicity

We looked for structures in a variety of molecular clouds and as a result our sample is not homogeneous for studying the binarity of a class of objects (like e.g. the CTTS). Moreover it is biased, among others, since some sources were known to be binary before our observations. However this sample does not present distinct overabundance of young binaries with respect to their main sequence counterparts as noticed by, e.g., Ghez et al. 1993 and Leinert et al. 1993.

Over the complete sample, the degree of multiplicity (number of multiple systems over the total number of sources) is 43$\pm$12% similar to what Leinert et al. (1993) found in Taurus. Caution should be taken in this comparison since the sample of Leinert contains only T Tauri stars and ours includes also some Herbig Ae/Be stars. The percentage increases to 56$\pm$18% if we consider only the T Tauri stars (18 in our sample). This result then becomes similar to the results of Duquennoy & Mayor (1991) for G dwarf primaries.

It is also interesting to note the absence of a significant difference between our percentage of multiplicity and the one found for all kinds of YSOs (polarized or not). This is not surprising since no correlation (Bastien 1996) could be found between the multiplicity of a source and its degree of polarization.

4.2. Color-color diagram

Fig. 8 is the J-H/H-K diagram for the sources of our sample for which the corresponding photometry and/or color indexes are available (see Tables 3 & 4). For each source, we have plotted the A and B component of the system together with a number from Table 1. The 3 σ uncertainty on the absolute value of the color indexes is estimated to be 0.4, while the relative uncertainty between the two components of a given system is lower (≈ 0.1).

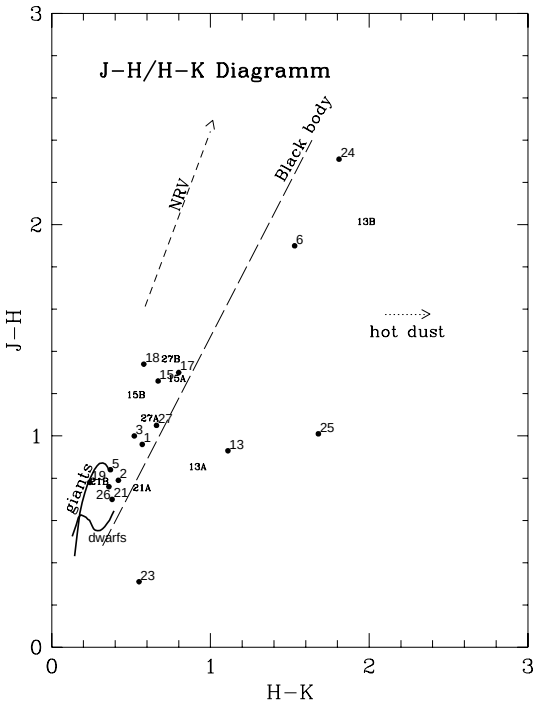

Fig. 8. J-H, H-K diagram for the studied sources. NRV represents the normal reddening vector. The numbers refer to the sources as indicated in column 1 of Table 1

Table 4. J-H, H-K colors: informations from the litterature.

Name	J-H	H-K	Reference
SZ Cha	0.96	0.57	Gauvin & Strom (1992)
LHα 332-20	0.79	0.42	Gauvin & Strom (1992)
HM 10	1.00	0.52	Prusti et al. (1992)
CED 110	0.84	0.37	Whittet et al. (1987)
Sz 21	1.9	1.53	Gauvin & Strom (1992)
ROX 16	1.3	0.8	Vrba et al. (1976)
ROX 31	1.34	0.58	this study
ROX 39	0.78	0.24	Walter et al. (1994)
ROX 43 AB	0.70	0.38	Walter et al. (1994)
ROX 43 A	0.74	0.51	Walter et al. (1994)
ROX 43 B	0.77	0.24	Walter et al. (1994)
AS 310	0.31	0.55	Berrilli et al. (1992)
R CrA	2.31	1.81	Hillenbrand et al. 1992
Parsamyan 21	0.76	0.36	Hillenbrand et al. 1992
V 536 Aql	1.05	0.66	Ageorges et al. 1994
V 536 Aql-A	1.07	0.56	Ageorges et al. 1994
V 536 Aql-B	1.35	0.69	Ageorges et al. 1994

Given the uncertainties, most of our sources fall in a region of the diagram that can be obtained by their position on the unredenned main sequence + giant locus and a normal reddening law. Still we note that sources like V536 Aql and Do-Ar 32 present significantly more reddening as a whole than other sources like ROX 43 suggesting more circumbinary obscuring material, if all objects come from the same locus.

Two objects in our sample present a clear intrinsic reddening: Do-Ar 24E, and VV CrA. For Do Ar 24E, for which we have relative measurements, the faintest component at 2.2 μm appears redder than the primary.

Infrared observations of pre-main-sequence binaries (e.g. Zinnecker 1989; Moneti & Zinnecker 1991) as well as numerical simulations (e.g. Bonnell & Bastien 1993) reported that

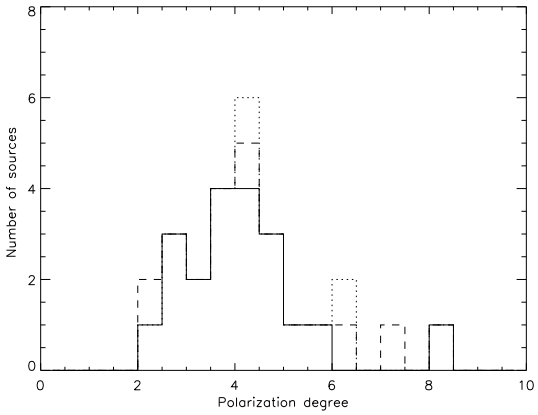

Fig. 9. Distribution of the sources of our sample as a function of the polarization degree. The full line is the distribution of the T Tauri stars. The Herbig Ae/Be stars are indicated by dotted lines. The dashed line represents the distribution of the sources with undetermined nature

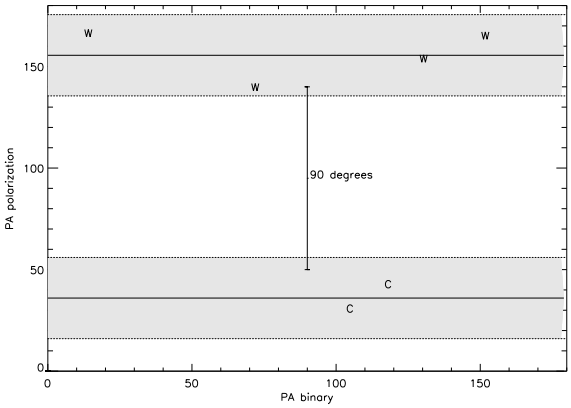

Fig. 10. Scheme representing the angle of intrinsic polarization as a function of the position angle of the binaries in the ρ Ophiuchius molecular cloud. The thin black horizontal lines represents the averaged position of WTTS (upper line) and CTTS (lower line) in this diagram. The grey areas corresponds to the respective error bars

Table 5. Polarization degree for sources in ρ Oph. The degree of polarization is given in% and the angle in degrees; 'obs' = observed, i.e. measured on the source, 'inter' = interstellar and 'intrins' = intrinsic, which is the presumed intrinsic degree of polarization of the source. The typical errors on the calculated instrinsic polarization are: ΔP_{IS} = 1% and $\Delta\theta_{IS}$ = 5°.

Source name	P_{obs}	θ_{obs}	P_{inter}	θ_{inter}	$\mathbf{P}_{intrins}$	$\theta_{intrins}$
WSB 16	2.36	160	2	40	3.8	-33.4
ROX 5	2.47	33	2.8	38	0.6	153.1
ROX 7	4.15	174.4	4	50	6.8	-21.9
Do Ar 21	5.81	1.5	4	55	8.1	-12.3
Do Ar 24E	4.59	179.9	4	55	7.1	164.4
ROX 14	7.13	25.8	3.2	43	4.9	14.4
ROX 16	4.07	30	3.2	30	0.9	30
Do Ar 32	5.3	39.7	3	38	2.3	42
ROX 30C	3.67	25.5	3	38	1.63	-1.2
ROX 31	4.88	56.4	4	58	0.9	139
ROX 43A	2.63	16	3.6	55	4.0	165.6

frequently the more luminous component is redder. Our sample is unfortunately too small to be able to recognize such an effect here. Larger samples of close binaries are needed to confirm this tendency.

4.3. Polarization

Fig. 9 represents the optical polarization distribution of our sample. This distribution is not characteristic of what has been observed so far for YSOs (e.g., Ménard and Bastien 1992; Bastien 1996). This is due to our selection criterion: we observed only sources with a large polarization. As a selection bias, we also find that the high polarization tail in this distribution is, as expected (Ménard and Bastien 1992), due to T Tauri stars.

One should however be cautious about the fact that the measurements given in Table 1 represent the observed polarization which is not necessarily the intrinsic one. To estimate the intrinsic polarization of our sources located in ρ Ophiuchus we considered the average values measured for a large number of background sources showing the same polarization with the same position angle. They have been considered as representative of the local interstellar polarization. We used measurements presented in Vrba et al. (1976) for background stars and we applied the correction formulae given by Goodrich (1986) and Wilking et al. (1980), assuming λ_{max} = 0.75μm. This procedure is statistical only and we get typical values of order ΔP_{IS} = 1% and $\Delta\theta_{IS}$ = 5^o.

The reliability of background stars' polarization to trace the interstellar magnetic field within molecular clouds has been questioned by Goodman (1996) for example. The grains deep inside the clouds may be less efficient polarizers. Since we don't know how deep in the clouds our sources are located, we may be correcting badly for the interstellar polarization fraction produced inside the cloud and we note that the intrinsic values we derive here may be affected by correspondingly larger errors locally.

Half of the sources in the sample have observed polarizations that are probably of interstellar origin based on a similarity of the position angle and the level of polarization with the interstellar values.

On the other hand, ROX 7, DoAr 21, and DoAr 24E have large intrinsic polarizations. This suggests the presence of circumstellar material. However, our observations do not reveal extended structures around any of these sources. A probable explanation is that the structures are too faint ($m_K < 12$) or too small ($\leq 0.2''$), thus escaping detection. Dust continuum measurements in the millimeter range would help solve that question.

In Fig. 10 we compare the projected position angle of the binary with the position angle of its polarization. The sample considered is small and the error bars are too large with respect to the intrinsic polarization of WTTS for example to draw any firm conclusions. However, we mention the trend of the 4 Weak-line T Tauris to show intrinsic polarization position angles close to $\sim 150^o$ while the two Classical T Tauris have position angles of $\sim 40^o$ instead. But to go further, much more data is needed.

A detailed study of the effects of the WTTS magnetic field on the nearby interstellar medium will be presented in Ageorges et al. (1997, in preparation).

4.4. Selection criteria

The selection of sources via their degree of polarization does not significantly lead to detection of extended sources. There are however many reasons to explain our lack of detection: either there is no circumstellar medium, or it is either too small for our resolution and/or too faint for our sensitivity. Moreover K band imaging might not be the best choice (small scattering efficiency) to look for extended structures seen in scattering.

Other studies were not more succesful finding a correlation between the degree of polarization and the nature of the source or its spectral type (Bastien 1996).

What seems more promising - and is under study - is the correlation between the degree of polarization and the radio activity of a source.

Acknowledgements. This work was part of the PhD thesis of N.A., who would like to thank L. Tacconi-Garman and R. Hofmann for their help and technical support at the telescope. We would also like to thank the ESO staff at La Silla and the CDS, France, for the SIMBAD data base, with which the bibliography has been realized. Many thanks also go to Ch. Leinert, R. O'Dell and H. Zinnecker for very fruitful discussions and comments. Finally we would like to thank the referee P. Bastien for his helpful remarks and suggestions.

References

Ageorges N., Ménard F., Monin J.L., Eckart A., 1994, A&A 283, L5
Ageorges N., Duschl W.J., 1996, Planetesimals around V536 Aql, In: Kress M.E., Tielens A.G.G.M., Pendleton Y.J. (eds.) NASA conference publication 3343, From Stardust to Planetesimals, p. 3-8
Ageorges N. et al., 1997, in preparation
Altenhoff W.J., Thum C., Wendkler H.J., 1994, A&A 281, 161-183
André P., Montmerle T., 1994, Ap. J. 420, 837-862
Bastian U., Mundt R., 1979, A&A Supp. Series 36, 57-60
Bastien P., Landstreet J.D., 1979, Ap J 229, L137
Bastien P., 1982, A&A Supp. Series 48, 153 & 513
Bastien P., et al., 1988, A.J., 95, 900
Bastien P., Ménard F., 1990, Ap. J. 364, 232-241
Bastien, P., 1996, Polarization of young stellar objects. In W.G. Roberge & D.C.B. Whittet (eds.) ASP Conf. Series 97, Polarimetry of the interstellar medium, p. 297
Berrilli F., et al., 1992, Ap.J. 398, 254-272
Bonnell I., Bastien P., 1993, Ap.J. 406, 614-628
Bouvier J., Appenzeller I., 1992, A&A Suppl. Series 92, 481-516
Chelli A., Zinnecker H., Carrasco L., Cruz-Gonzalez I., Perrier C., 1988, A&A 207, 46
Cohen M., Kuhi L.V., 1979, Ap. J. Supp. Series 41, 743-843
Duquennoy A., Mayor M., 1991, A&A 248, 485
Eckart A., Duhoux P.R.M., 1990, In Elston R. (ed) ASP Conf. Series, Astrophysics with infrared arrays p. 336
Eckart A., Genzel R., 1997, MNRAS 284, 576
Feigelson E.D., Kriss G.A., 1989, Ap. J. 338, 262-276
Fich M., Treffers R.R., Dahl G.P., 1990, A.J. 99, 622
Finkenzeller U., Mundt R., 1984, A&A Supp. Series 55, 109-141
Gauvin L.S., Strom K.M., 1992, A.J. 385, 217
Georgelin Y.P., Georgelin Y.M., 1970, A&A 6, 349
Ghez A.M., Neugebauer G., Matthews K, 1993, A.J. 106, 2005
Goodman A. A., 1996, The interpretation of polarization position angle measurements. In W.G. Roberge & D.C.B. Whittet (eds.) ASP Conf. Series 97, Polarimetry of the interstellar medium, p. 325
Goodrich R.W., 1986, Ap.J. 311, 882
Goodrich R.W., 1993, Ap.J. Suppl. Series 86, 499
Henning T., Launhardt R., Steinacker J., Thamm E., 1994, A&A 291, 546-556
Hillenbrand L.A., Strom S.E., Vrba F.J., Keene J., 1992, Ap.J. 397, 613-643
Hofmann R., Brandl B., Eckart A., Eisenhauer F., Tacconi-Garman L.E., In A.M. Fowler (ed) SPIE International Symposium 2475, Infrared Detectors and Instrumentation for Astronomy, p. 192
Hunter D.A., Thronson H.A. Jr., Wilton C., 1990, A.J. 100, 1915
Leinert Ch. et al., 1993, AA 278, 129
Mathieu R.D., Walter F.M., Myers P.C., 1989, A.J. 98, 987
Ménard F., Bastien P., 1992, A.J. 103, 564
Menten K.M., Reid M.J., Eckart A., Genzel R., Feb. 1997, ApJ, in press
Merrill P.W., Burwell C.G., 1950, Ap.J. 112, 72
Moneti A., Zinnecker H., 1991, A&A 242, 428-432
Montmerle T., Koch-Miramond L., Falgarone E., Grindlay J.E., 1983, Ap.J. 269, 182-201
Palla F., Prusti T., 1993, A&A 272, 249
Prusti T., Whittet D.C.B., Wesselius P.R., 1992, MNRAS 254, 361
Reipurth B., Zinnecker H., 1993, A&A 278, 81
Schwarz H.E., 1989, ESO Operating Manual No.13
Simon M., et al., 1987, Ap.J. 320, 344
Simon M., et al., 1995, Ap.J. 443, 625
Skinner S.L., Brown A., Stewart R.T., 1993, Ap.J. Supp. Series 87, 217-265
Stenholm B., Acker A., 1987, A&A Supp. Series 68, 51-62
Vrba F.J., Strom S.E., Strom K.M., 1976, A.J. 81, 958
Walter F.M., 1992, A.J. 104, 758-761
Walter F.M., Vrba F.J., Mathieu R.D., Brown A., Myers P.C., 1994, A.J. 107, 692
Whittet D.C.B., et al., 1987, MNRAS 224, 497
Wilking B.A., Lebofsky M.J., Martin P.G., Rieke G.H., Kemp J.C., 1980, ApJ 235, 905
Zinnecker H., 1989, In B. Reipurth (ed), Low mass star formation and pre-main-sequence objects, p. 447

This article was processed by the author using Springer-Verlag LaTeX A&A style file *L-AA* version 3.